

Coated Conductor technology for the beamscreen chamber of future high energy circular colliders

T Puig¹, P Krkotic^{2,3}, A Romanov¹, J O'Callaghan³, D. A. Zanin⁴, H. Neupert⁴, P C Pinto⁴, P Demolon⁴, A Granadeiro Costa⁴, M Taborelli⁴, F Perez², M Pont², J Gutierrez^{1†}, S Calatroni⁴

¹ Institut de Ciència de Materials de Barcelona, C.S.I.C., Campus U.A. Barcelona, 08193 Bellaterra, Catalonia, Spain

² ALBA Synchrotron - CELLS, Carrer de la Llum 2-26, 08290 Cerdanyola del Vallés (Barcelona), Spain

³ Universitat Politècnica de Catalunya. CommSensLab. c/ Jordi Girona 1 08034 Barcelona, Catalonia, Spain

⁴European Organization for Nuclear Research (CERN), 1211 Geneva 23, Switzerland

† e-mail: jgutierrez@icmab.es

Abstract. The surface resistance of state-of-the-art REBa₂Cu₃O_{7-x} coated conductors has been measured at 8 GHz versus temperature and magnetic field. We show that the surface resistance of REBa₂Cu₃O_{7-x} strongly depends on the microstructure of the material. We have compared our results to those determined by the rigid fluxon model. The model gives a very good qualitative description of our data, opening the door to unravel the effect of material microstructure and vortex interactions on the surface resistance of high temperature superconductors. Moreover, it provides a powerful tool to design the best coated conductor architecture that minimizes the in-field surface resistance. We have found that the surface resistance of REBa₂Cu₃O_{7-x} at 50 K and up to 9 T is lower than that of copper. This fact poses coated conductors as strong candidate to substitute copper as a beamscreen coating in CERN's future circular collider. To this end we have also analysed the secondary electron yield of REBa₂Cu₃O_{7-x} and found a compatible coating made of sputtered Ti and amorphous Carbon that decreases the secondary electron yield close to unity, a mandatory requirement for the beamscreen chamber of a circular collider in order to prevent the electron-cloud phenomenon.

1. Introduction

On the 4th of July of 2012 scientists at CERN announced the discovery of the Higgs boson based on collisions detected in the ATLAS and CMS detectors in the LHC. The Higgs boson is responsible for the origin of mass of subatomic particles, and is an essential component of the Standard Model, one of the most successful theoretical frameworks in physics. Thanks to this discovery, on the 10th of December of 2013 F. Englert and P. Higgs were awarded the Nobel Prize in Physics for their theoretical prediction in 1964. The large hadron collider (LHC) has proven fundamental to the advanced of our knowledge of matter and the Standard Model. However, the 13 TeV center-of-mass collisions it produces cannot explore newer key questions about the Universe, such as dark matter, dark energy, supersymmetry, the origin of neutrino masses, or the existence of extra dimensions. To this end, the future circular collider (FCC-hh) design study explores options for a next generation of hadron-hadron collider which should succeed the LHC at the end of its productive life. The FCC-hh aims at 100 TeV center-of-mass proton-proton collision energy in a 100 km circumference ring located near the CERN site [1]. Superconducting magnets cooled at 1.9 K and generating 16 T will steer the proton beam, which will emit 28 W/m/beam of synchrotron radiation. A stainless steel beamscreen held at around 50 K will shield the magnets from it, thus allowing for a better overall cryogenic efficiency and power consumption. The beamscreen is directly seen by the proton beam, therefore it must present a low secondary electron yield and should minimize the beam impedance. A similar beamscreen, held at temperatures between 5 K and 20 K, in the presently running LHC makes use of a copper coating to minimize the impedance due to the beam image currents [2]. However the surface resistance of copper at 50 K might not be sufficiently low to ensure stable operation of the FCC-hh. The goal of this paper is to present the first experimental results on the possible use of REBa₂Cu₃O_{7-x} coated conductors (REBCO CCs, RE = Y, Gd) [3] as coating materials for the beamscreen chamber in order to minimize the beam impedance [4].

The operating conditions of REBCO CCs in the FCC-hh are extremely challenging. The beam screen will operate at a temperature range between 40 K and 60 K, and the coating shall remain superconducting up to a field of 16 T. The average beam current in the FCC-hh is of the order of 0.6 A and will be distributed in proton bunches 8 cm long, producing image currents per bunch as high as 25 A, with a frequency spectrum extending above 1 GHz [5]. If the coating is about 1 μ m thick; the critical current density will have to be higher than 25 kA/cm² at 50 K and 16 T. On top of that, the surface resistance has to be better than copper for all the frequency, temperature and magnetic field ranges of FCC-hh's operating conditions.

In order to assess if REBCO CCs can provide the desired solution for the demanding conditions in the beamscreen chamber, we must study their superconducting and mechanical properties under these conditions, and assess their compatibility with the demands of a high energy circular collider.

2. Materials and methods

We have performed a study of the surface resistance and material compatibility for six different REBCO CCs, see Tab. 1, conditions close to those found in the FCC-hh. The CCs have been provided by Bruker, Fujikura, Sunam, SuperOx, SuperPower and Theva. For this study, we have stripped both the Cu and Ag layers from the CC, so that the REBCO layer is exposed to the RF fields. The removal process of the Ag and Cu layers has been done using a solution 1:1:20 of $\text{NH}_3:\text{H}_2\text{O}_2:\text{Methanol}$.

	Rare-earth	Nano-Inclusions	REBCO thickness (μm)	Growth method
Bruker	Y	BaZrO_3	1.6	DD - PLD
Fujikura	Gd	none	1.8	PLD
Sunam	Gd	none	1.6	RCE - DR
SuperOx	Gd	none	0.9	PLD
SuperPower	Y,Gd	BaZrO_3	1.5	MOCVD
Theva	Gd	none	3	EB - PVD

Table 1. Coated conductor architecture for the different providers. The different growth methods are pulsed laser deposition (PLD), double disordered REBCO layer by PLD (DD - PLD) reactive co-evaporation by deposition and reaction (RCE - DR), metalorganic chemical vapor deposition (MOCVD) and electron-beam physical vapor deposition (EB - PVD)

The characterization of the critical current density (J_c) has been performed by means of vibrating sample magnetometry. The characterization of the normal to superconducting transition temperature (T_c) and the normal state resistivity of the REBCO layer has been carried out by electrical transport in the Van der Pauw geometry. Vibrating sample magnetometry and electrical transport characterization has been performed with a Quantum Design's PPMS[®] equipped with a 9 T magnet. Figures 1(a) and 1(b) show the critical current per centimeter width $I_c - width(\text{B}, 50 \text{ K})$ and $\rho(\text{T})$ curves for the different providers. During operation, the beamscreen will face peaks of image currents up to 25 A, taking into account the designed beamscreen chamber dimensions [1], it translates into $I - width \approx 3 \text{ A/cm}$. We have no access to characterization at 16 T, but it can be inferred from Fig. 1(a) that the $I_c - width$ of most of the providers will easily fall above this threshold.

We have used a microwave, non-destructive, dielectric resonator (DR) technique [6] to characterize the surface resistance (R_s) of different CCs. The DR has been redesigned from that used in [7, 8, 9] to meet the sensitivity requirements for the characterization of CCs as a function of temperature (5 - 300 K) and magnetic fields up to 9 T in a PPMS. R_s data points of in-field measurements were acquired in field-cooled mode. The DR uses a rutile (TiO_2) single crystal disk operating at 8 GHz in the TE011 mode at 50 K. The resonator is shielded axially by the two samples to be examined. The measured quality factor values, which describe the influence of the absorption on the resonator

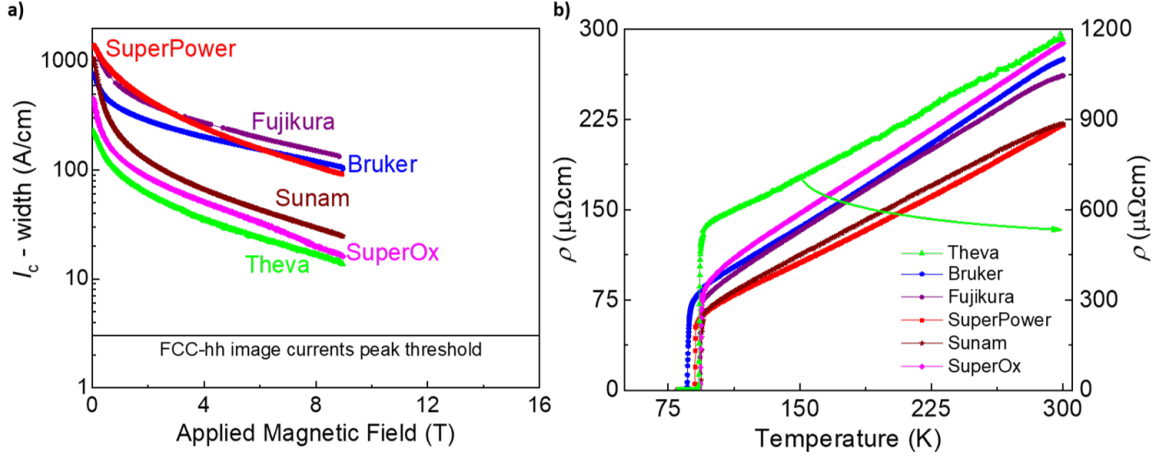


Figure 1. Magnetic field dependence of $I_c - width$ at 50 K (a) and temperature dependence of the resistivity at zero applied magnetic field (b) for the different providers.

modes, can be directly related to the overall surface resistance as:

$$\frac{1}{Q_0} = \frac{R_s^1}{G^1} + \frac{R_s^2}{G^2} + \frac{R_s^3}{G^3} + p \cdot \tan(\delta) \quad (1)$$

where R_s^1 and R_s^2 are the surface resistances of the CCs being investigated and R_s^3 is the surface resistance of the metallic enclosure. Respectively, the geometrical factors G^1 and G^2 refer to the upper and lower samples, and G^3 refers to the lateral surface of the resonator cavity. The last term of the equation describes the filling factor p and the loss tangent $\tan(\delta)$ of the rutile. As a result of using equal samples as endplates in the measurements, $R_s^1 = R_s^2$ and $G^1 = G^2$, and knowing that the losses of the metallic housing wall can be neglected in this geometry ($\frac{R_s^3}{G^3} \approx 0$) [9], we can rewrite Eq. (1) for the DR used in this work as:

$$R_s(T, B) = \frac{G}{2} \cdot \left[\frac{1}{Q_0(T, B)} - p \tan(\delta) \right] \quad (2)$$

where G is the geometrical factor of the measured CCs. This factor can be calculated using the analytical expressions for the electromagnetic fields given in [10, 11]. The resulting value was confirmed through measurements of the quality factor for different configurations of normal metals of known conductivity as described in [9] and, in addition, it was computed using a finite element analysis simulation. The geometrical factor obtained with the three methods showed good agreement.

3. Surface resistance of coated conductors

The surface resistance as a function of the temperature at zero magnetic field for the six different providers of CCs is shown in Fig. 2. We have included the R_s of 300 μm thick Cu co-laminated on stainless steel from CERN for comparison purposes, as it

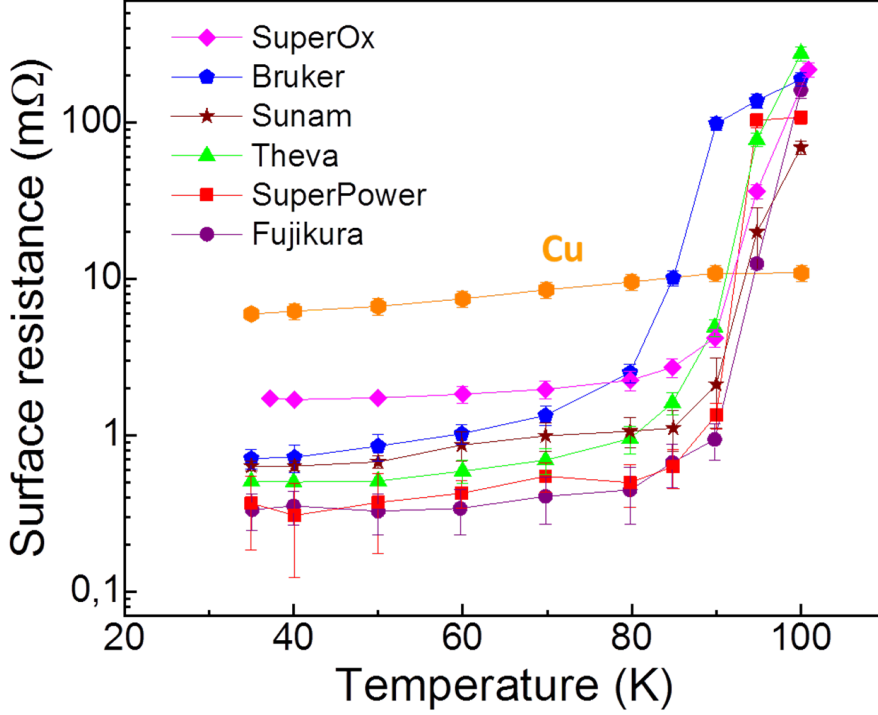


Figure 2. Temperature dependence of the surface resistance at 8 GHz and zero applied magnetic field. Below T_c , CCs' R_s outperforms that of copper.

is intentionally proposed for the FCC-hh's beam-screen chamber. All CCs but that of Bruker show a T_c around 90 K. Bruker's double disordered REBCO layer slightly sacrifices performance at high temperatures to optimize superconducting properties at 4.2 K and high magnetic fields. Above T_c , CCs show a high R_s value. Note that in the normal state REBCO has a high resistance, at 8 GHz and 100 K the skin depth of REBCO is $\lambda' \approx 6 \mu\text{m}$, which is higher than REBCO layer thickness. Therefore, the value of R_s we observe above T_c is strongly influenced by the metallic substrate of the CC (stainless steel or hastelloy). Below T_c the skin depth of the RF field is of the order of the superconducting penetration depth λ [12], much smaller than the thickness of the superconducting layer of the CCs. Therefore, below T_c the R_s values we observe are those of the REBCO superconducting state. At zero applied magnetic field, we observe that R_s of CCs in the superconducting state is much lower than that of copper. In particular, at 50 K, CCs outperform copper by an order of magnitude. The error bars of the R_s values for the different CCs shown in Fig. 2 have been obtained after a careful analysis of the error sources (see the supplementary information). From this analysis we have determined that the error we commit in the determination of the values of R_s for the different CC providers is at maximum $\approx 10\%$.

The surface resistance of a superconductor can be expressed in general terms by the following expression [5]:

$$R_s(H_{rf}, T, B) = R_{BCS}(H_{rf}, T) + R_{res}(H_{rf}) + R_{fl}(H_{rf}, T, B) \quad (3)$$

The first term on the right hand side of Eq. (3) is the surface resistance as derived from the BCS theory for traditional low-temperature superconductors. For those materials, the results match very well with experimental data. However, the derivation of this term for high temperature superconductors, such as REBCO CCs, faces several difficulties [13]. The second term on the right hand side of Eq. (3) is the residual surface resistance, independent of magnetic field and temperature. There is no theory that successfully describes this term and is left to be determined experimentally. Its origin is usually attributed to material defects, such as grain boundaries, twin boundaries, or dislocations occurring naturally in CCs. Finally, the term R_{fl} accounts for the dissipation arising from the movement of trapped vortices inside the superconductor and is the relevant term at high magnetic fields and for the work presented here. Some theoretical frameworks, based on a rigid fluxon model, successfully account for the temperature and magnetic field dependence of R_s arising from this term, see [14] and references therein. Fig. 3 shows the surface resistance for the six different coated conductors at 50 K and as a function of the applied magnetic field. The magnetic field is applied along REBCO's c-axis for all but Theva's CC as we will discuss below. Copper is also represented for the sake of comparison. It is clear that as opposed to the metal, the R_s of a superconductor is strongly influenced by the presence of a magnetic field.

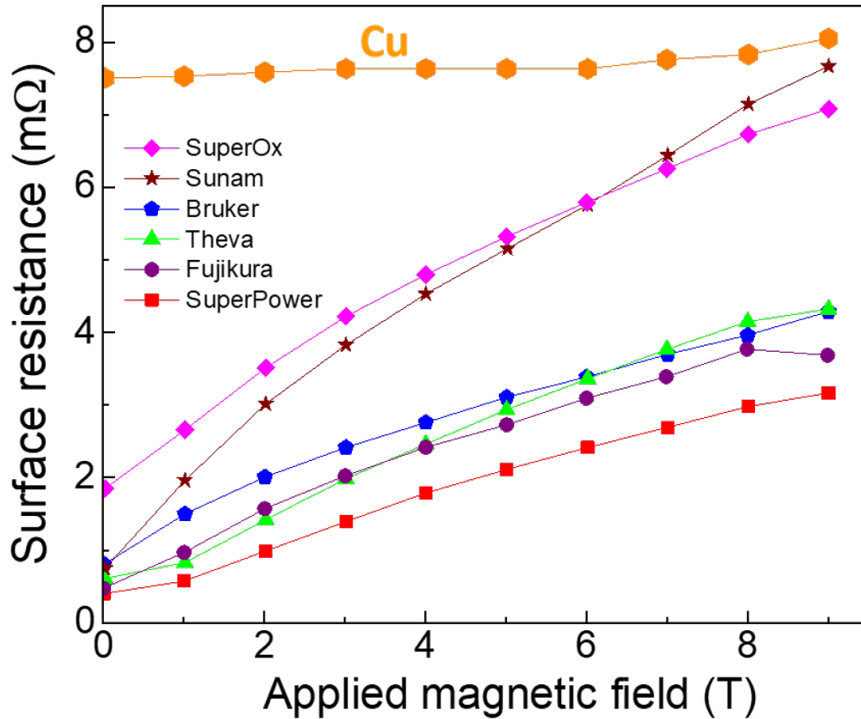


Figure 3. Magnetic field dependence of the surface resistance at 8 GHz and 50 K. Up to 9 T, CCs' R_s outperforms that of copper.

Fig. 3 shows that we can divide the $R_s(B)$ of CCs in two groups. The first group, includes CCs with a R_s showing a steeper magnetic field dependence. The materials belonging to this group are REBCO CCs which $J_c(B)$ shows also a steeper magnetic

field dependence (specially at low magnetic fields). This is observed in Fig. 1 a). The second group includes CCs which R_s has a weak magnetic field dependence and widely outperforms copper's R_s up to 9 T. Within this group, we find CCs which $J_c(B)$ also shows a weak dependence with the magnetic field (see Fig. 1 a)). The providers of CCs follow different strategies to achieve this weak dependence of $J_c(B)$. REBCO grown by SuperPower and Bruker includes BaZrO₃ nanorods in the REBCO matrix which prove very effective vortex pinning centers. It is worth mentioning that YBCO grown by Bruker presents, additionally, a double-disordered matrix very effective at pinning vortices at low temperatures. Fujikura's CCs present a high J_c (self field) in combination with a weak magnetic field dependence as a result of an intrinsic disorder very efficient at pinning vortices. In this group we also find the Theva inclined substrate technology CC [15] (see Tab. 1). Theva inclined substrate technology has two main implications regarding $R_s(H_{rf}, T, B)$. On the one hand, the applied magnetic field during the experiments is not directed along the REBCO's c-axis, but is tilted by $\theta = 24^\circ$ away from it [16]. Due to the anisotropic nature of REBCO, this translates into the superconductor being exposed to an effective magnetic field along the c-axis (B_{eff}^c) which is lower than the applied one according to $B_{eff}^c = \epsilon(\theta, \gamma)B$ [17], where $\epsilon(\theta, \gamma) = \sqrt{\cos^2(\theta) + \frac{1}{\gamma^2} \sin^2(\theta)}$ and γ is the material electronic anisotropy, which for REBCO ranges between 5 - 8. In the case of Theva CCs $B_{eff}^c \approx 0.9B$. On the other hand, the tilted c-axis nature of the material gives rise to a higher normal state resistivity as observed in Fig. 1(b). The reason for this resides again on the intrinsic electronic mass anisotropy of REBCO, as electrons flowing along the c-axis have a higher effective mass as those flowing along the ab-planes. Interestingly, the rigid fluxon model predicts that a higher normal state resistivity may translate into a lower R_s of the superconductor in the presence of a magnetic field. The results shown in Fig. 3 imply that the R_s of a superconductor under the presence of a magnetic field is strongly dependent on the CCs microstructure.

Although state-of-the-art CCs already outperform copper under the aforementioned conditions, these results open the door to study the possibility to engineer CC's microstructure to optimize its $R_s(H_{rf}, T, B)$ for the specific conditions found in a high energy circular collider such as the CERN's FCC-hh. In order to understand the most effective material parameter, we have applied the rigid fluxon model [14] to the measured data. The model relates $R_{fl}(T, B)$ to superconducting properties such as J_c , T_c , upper critical field (B_{c2}), or the penetration depth λ . In Fig. 4(a) we show the $R_s(B)$ at 50 K for the different CCs determined by the rigid fluxon model (see supplementary information). We have fed into the equation the measured values for each CC of their J_c , T_c and normal state resistivity (see Fig. 1). We have derived λ at 50 K from the two fluid model expression using $\lambda(0) = 150$ nm for REBCO [18]. We have derived B_{c2} from resistivity measurements as a function of temperature and magnetic field as described in [19]. The values we obtain of B_{c2} are in agreement previous reports [20]. We observe that the model accurately predicts the magnetic field dependence of R_s for each provider but it overestimates the R_s values. Comparing Fig. 3 with Fig. 4(a), it

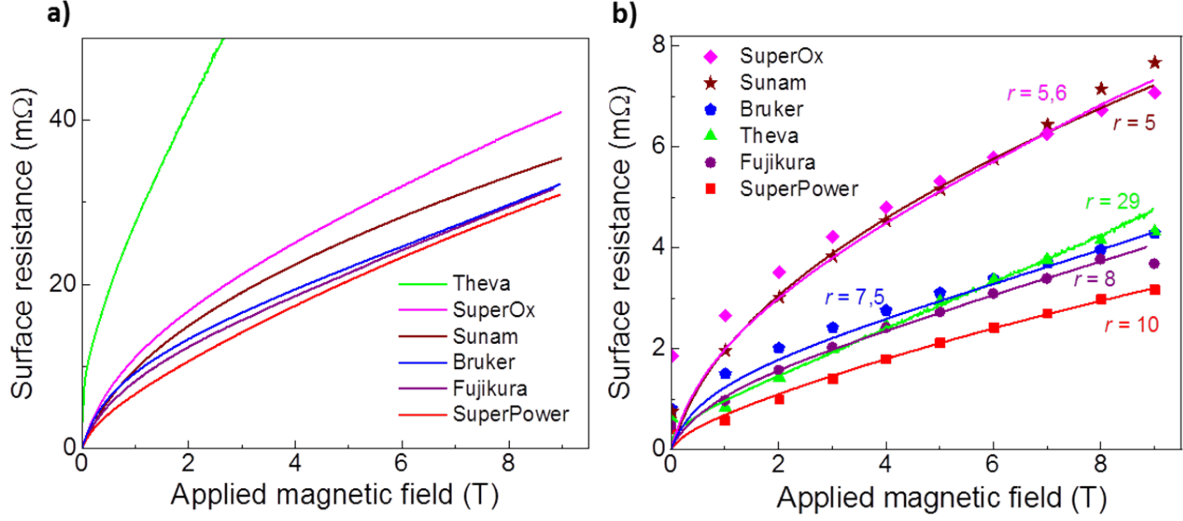


Figure 4. Magnetic field dependence of the surface resistance for the different CCs at 8 GHz and 50 K. (a) $R_s(B)$ derived from the rigid fluxon model using using Eq. S1 of supplementary information. (b) solid symbols represent the experimental values of $R_s(B)$ and solid lines fits using Eq. (S3) of supplementary information. The values of the fitting parameter r are included for each provider.

is worth noting that, besides Theva, the model also predicts correctly the ranking of CCs. In Fig. 4(b) we use a modification of Eq. 11 found in reference [14] to fit our data (see supplementary information) that includes a scaling factor r to treat the data with only one fitting parameter (see Eq. (S3) in the supplementary information). It can be observed that the matching is very good, except at lower fields. This can be expected since the fit accounts for the term $R_{fl}(T, B)$ of Eq. (3), and it is at high fields where R_s will be dominated by R_{fl} . Therefore, it is evidenced that this approach can be used as a tool to link superconducting properties of the material (ρ_n, T_c, B_{c2}, J_c) to $R_s(T, B)$. Therefore, the model serves as a bridge between $R_s(T, B)$ and CC's microstructure.

We have shown in Fig. 4 that, under the conditions of our experiments, the rigid fluxon model overestimates the real value of R_s of the CCs by a factor $r \approx 5 - 10$. In the particular case of Theva's inclined substrate technology, this factor is 29. There are several potential sources for the disagreement between theory and experiment, but most arguably the rigid fluxon model uses two strong hypothesis: (i) vortices behave as rigid flux lines which do not bend or break and (ii) the vortex lattice cannot deform. These are two very strong statements that can be valid for some low temperature superconductor and very thin films, but do not accurately describe the vortex physics of high-temperature superconductors, specially at temperatures of 50 K and in the case of CCs with strong artificial pinning centers. Hypothesis (i) implies that a vortex will move as a whole entity when it is depinned. The CCs we have studied have thicknesses ranging 1 - 3 μm (see Tab. (1)), while the currents induced by the H_{rf} in our experiments circulate within a thickness in the range of $\lambda(50\text{ K}) \approx 160\text{ nm}$. This translates into a force acting on the vortex that is not homogeneous along its length. Therefore, it is

expected that under this scenario, a strongly pinned vortex will depin inhomogeneously along its length and bending modes of fluxon will also play a strong role. Similarly, hypothesis (ii) implies that if a vortex moves, the whole lattice moves together in the same way. This scenario is highly unlikely in a CC, specially in CC including artificially engineered pinning landscapes. CCs with artificial pinning centers have a very complex pinning landscape composed of weak and strong pinning centers [21]. Therefore, at a local scale, above fields not too large (≈ 0.1 T at 50 K) different vortices will be under the effect of different pinning force intensities, as some vortices will be strongly pinned by nanorods, others may be partially pinned by several weak pinning centers, and others will be interstitially pinned. The fact that the scaling factor r is smaller for CCs with a steeper $J_c(B)$ than for those with a smoother $J_c(B)$ dependence, points in the direction of our reasoning. Nevertheless, we have to further conduct studies in this regard to better understand this disagreement between the model and the experiment.

Even though the working conditions arising at the FCC-hh are not yet within our experimental reach, the obtained data combined with the rigid fluxon model can be used to describe the trend of the CCs behaviour at lower frequencies and higher magnetic fields. According to the rigid fluxon model, the dependence of R_s on ν is steeper than the dependence on B , $R_s(\nu, B) \approx \sqrt{B}(\frac{\nu}{\nu_0})^{3/2}$, where ν_0 is the depinning frequency, which depends on the pinning strength and fluxon viscosity [22] and therefore it is temperature, magnetic field and material dependent [23, 24, 25]. For the REBCO CCs analyzed in this work we have estimated the values of $\nu_0 \approx 1 - 3$ GHz at 50 K and 9 T according to Eq. (S2) in the supplementary information; We observed that CCs containing artificially engineered pinning centers have the highest ν_0 amongst studied CCs. We have shown that the predicted $R_s(B)$ behaviour is in excellent agreement with our experimental $R_s(B)$ curves at 50 K, which show only a weak dependence with the magnetic field $\approx \sqrt{B}$. Consequently, based on the mentioned assumptions, REBCO CCs may outperform copper's R_s by a factor 5 under the FCC-hh conditions.

4. Secondary electron yield of coated conductors

The build up of secondary electrons is a common barrier to overcome in designing high-energy particle accelerators. A secondary electron yield (SEY) well above unity is likely to generate electron clouds inside the beam-screen chamber which can be catastrophic for the stability of the proton beam. The SEY of a material is defined as the number of secondary electrons emitted from one incident electron. For this reason, among other challenges, we have to study the secondary electron yield of REBCO. Seed electrons, for example photo-electrons generated from synchrotron radiation hitting the walls of the beam-screen chamber, can be slingshot by the proton bunches back into the walls. In turn, these electrons will excite more electrons if the SEY of the wall (REBCO in our case) is high enough. This results in a positive feedback loop which produces a cascade effect [26]. These free electrons will be attracted by the proton bunches generating an electron cloud around the protons, highly disrupting the proton beam.

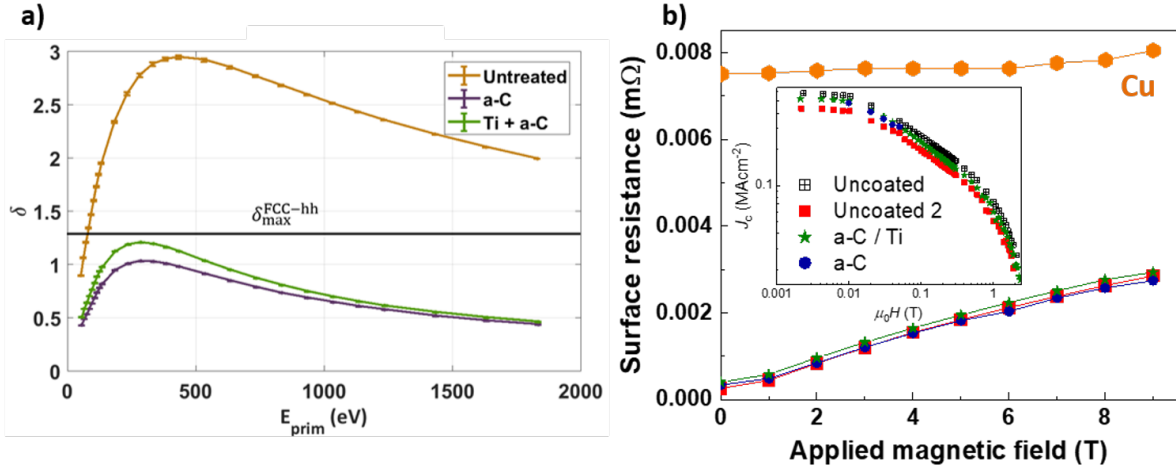


Figure 5. (a) Secondary electron yield of uncoated and a-C coated REBCO layers. The horizontal line depicts the maximum SEY allowed for a material to work in the FCC-hh. (b) $R_s(B)$ at 50 K of CCs uncoated and coated with 50 nm a-C and with 50 nm a-C and 100 nm of Ti (the legend is shared with that of the inset). In orange hexagons we show the $R_s(B)$ of copper. The inset shows the $J_c(B, 77 K)$ for the uncoated and a-C coated CCs.

Other consequences of secondary electron multiplication are dynamic pressure rises and thermal load in cryogenic vacuum systems [27].

The SEY of different REBCO CCs is measured in a customized SPECS UHV system (base pressure of $2 \cdot 10^{-9}$ mbar) of the TE-VSC group at CERN. The SEY operational vacuum chamber consists of an electron gun (ELG-2/EGPS-1022 from Kimball Physics) and a revolving sample holder. SEY is measured in two consecutive steps. In the first step the CC samples are positively biased (nominal +45 V). Primary electrons - of variable energies (E_{prim}) between 100 and 1800 eV impinge with normal incidence on the surface and generate secondary electrons. All secondary electrons are collected by the sample. We define this sample current to be the current of the primary electrons (I_{pe}). In the second step, the CC samples are negatively biased (nominal -45 V). All secondary electrons generated by the primary electron beam leave the sample. We define this sample current as the absorbed current (I_{abs}). Hence, the SEY (δ) can be determined by $\delta = \frac{I_{pe} - I_{abs}}{I_{pe}}$. δ is averaged over three different spots in the center of the sample. In Fig. 5(a), we observe that the SEY value for plain REBCO exposed to air is above a horizontal line at $\delta \approx 1.3$, the limit imposed for a material by CERN in order to operate inside the FCC-hh beam-screen chamber [1].

In recent years, CERN has developed extensive know-how in SEY reduction by different surface treatments. Bombardment with electrons of few hundred eV to clean the surface, or deposition of a thin layer of either amorphous carbon (a-C) or non-evaporable getter are typical ways to lower the SEY [27, 28]. Contrary to a-C deposition, non-evaporable getter coating requires a thermal treatment around 200 °C in UHV [29]. Therefore, among the potential cures for low SEY, a-C on a sample surface seems to be one of the most promising candidates for REBCO layers due to its convenient and

non-damaging deposition. We coated REBCO CCs with a 50 nm thick a-C layer, in a cylindrical UHV chamber at a pressure ranging between $1 \cdot 10^{-6} - 3 \cdot 10^{-5}$ mbar by means of dc magnetron sputtering deposition using a graphite rod as the target and Ar as the sputter gas, at a deposition rate of 0.5 nm/min. Moreover, a second layer architecture with Ti sandwiched between REBCO and a-C was produced. Ti as an interlayer increases on the one hand the adhesion between the top and bottom layers and on the other hand acts as a getter for possible a-C contaminants [30]. The deposited film thickness have to account for a compromise between low SEY and low R_s . It was chosen to be 50 nm and 100 nm for the a-C and Ti layers respectively. The SEY for a representative coated REBCO layers is shown in Fig. 5(a) (other CCs from this study showing similar results). In both cases, the maximum SEY δ_{max} is reduced below the acceptable threshold δ_{max}^{FCC-hh} . In the inset to Fig. 5(b) we show $J_c(B)$ at 77 K of a CC before and after coating it with a-C and a-C and Ti. $J_c(B)$ has been determined from magnetization measurements using the Bean critical state model [31]. No deterioration of $J_c(B)$ is observed. Similarly, in Fig. 5(b) we present the R_s dependence with the magnetic field at 50 K of a CC before and after coating it with a-C. We observe no degradation of the $R_s(B)$ values for the sample coated with a-C and only a slight increase is appreciated for the sample coated with a-C /Ti. At the frequency of 8 GHz and 50 K, the skin depth of a-C is $\lambda' \approx 23 \mu\text{m}$ and that for Ti is $\lambda' \approx 1 \mu\text{m}$. Therefore, the slight increase of the surface resistance found in the samples coated with a a-C /Ti bi-layer is ascribed to the loss introduced by the 100 nm thick metallic Ti layer. Therefore, we demonstrate that a sputtered a-C layer is a good solution to lower δ_{max} down to levels compatible with the FCC-hh requirements without any significant degradation of $J_c(B)$, T_c or R_s in the REBCO layer.

5. Conclusions

We present the first experimental evidence that REBCO CCs are true potential candidates to substitute copper as the coating for the beam-screen chamber of future high energy circular colliders such as the FCC-hh in CERN or the super proton-proton collider by CAS- IHEP in China. We have found that at 8 GHz and 50 K, the surface resistance of REBCO CCs outperforms that of copper up to 9 T. Our results clearly show that REBCO's $R_s(B)$ strongly depends on the material micro- (and nano-) structure.

In addition, we have assessed a possible source of beam instabilities arising from the generation of electron clouds within the beam-screen chamber. While REBCO surface chemistry is unsuitable due to its high secondary electron yield, we have demonstrated that it is possible to deposit a thin layer of amorphous carbon to reduce the SEY down $\delta_{max} = 1.03$, complying with the FCC-hh demands of $\delta_{max}^{FCC-hh} = 1.3$.

In this study we have used the rigid fluxon model to describe our results, finding a very good qualitative description of the magnetic field dependence of R_s . While our initial results are limited to 9 T, well below the 16 T to be found in the FCC-hh, our R_s measurements are performed at a frequency of $\nu = 8$ GHz, much higher than

the expected beam frequency spectrum of the FCC-hh. According to the rigid fluxon model this plays in great advantage for REBCO's $R_s(B)$. Based on the predictions of the rigid fluxon model, under the FCC-hh working conditions, REBCO's R_s may outperform copper's R_s by at least a factor 5. Nevertheless, the model fails to give accurate quantitative values of REBCO's R_s . We have introduced an overall correction factor r that roughly correlates with the pinning strength of the CC (i.e. r is larger for CCs that show a smooth dependence of the J_c with the magnetic field). A deeper understanding of this correction factor will allow us to relate superconducting properties accessible by conventional measurement techniques to R_s and open an important door to relate REBCO's microstructure to its R_s . In that way it will be possible to envision a CC architecture that minimizes R_s at the desired working conditions of the application.

6. Acknowledgements

Authors acknowledge the support and samples provided by Bruker, Fujikura, Sunam, SuperOx, SuperPower and Theva. Authors acknowledge CERN funding FCC-GOV-CC-0073/1724666/KE3359, MAT2014-51778-C2 COACHSUPENERGY, 2017-SGR 1519 from Generalitat de Catalunya and COST Action NANOCOHBRI (CA16218). ICMAB authors acknowledge the Center of Excellence award Severo Ochoa SEV-2015-0496 and its Future Interdisciplinary Projects action. A. R acknowledges MSCA-COFUND-2016-754397 and J. G acknowledges MSCA-COFUND-2014-665919 for financial support. The authors would like to acknowledge Prof. Ruggero Vaglio from University of Naples Federico II for the useful discussions on the rigid fluxon model.

7. References

- [1] Benedikt M, Capeans Garrido M, Cerutti F, Goddard B, Gutleber J, Jimenez J M, Mangano M, Mertens V, Osborne J A, Otto T, Poole J, Riegler W, Schulte D, Taviani L J, Tommasini D, Zimmermann F, Future Circular Collider Study. Volume 3: The Hadron Collider (FCC-hh) Conceptual Design Report, preprint edited by M. Benedikt et al. CERN accelerator reports, CERN-ACC-2018-0058, Geneva, December 2018. Submitted to Eur. Phys. J. ST.
- [2] Ruggiero F, 1995 Part. Accel. 50 83
- [3] Obradors X and Puig T 2014 Supercond. Sci. Technol. 27 044003
- [4] Krkotić P, Niedermayer U and Boine-Frankenheim O 2018 Nuclear Instruments and Methods in Physics Research Section A: Accelerators, Spectrometers, Detectors and Associated Equipment 895 56-61
- [5] Calatroni S, 2016 IEEE Trans. Appl. Supercond. 26 3500204
- [6] Klein N, Zuccaro C, Dähne U, Schulz H and Tellmann N, 1995 J. Appl. Phys. 78 6683
- [7] Mateu J, Collado C, Menendez O and O'Callaghan J M, 2003 Journal of Superconductivity: Incorporating Novel Magnetism 16 873
- [8] Mateu J, Collado C, Menendez and O'Callaghan J M, 2003 Appl. Phys. Lett. 82 97 - 99
- [9] Krkotić P, Aguasca A, O'Callaghan J M, 2018 48th European Microwave Conference DOI:10.23919/EuMC.2018.8541442
- [10] Padamsee H, Knobloch J and Hays T, 1998 RF Superconductivity for Accelerators (John Wiley and Sons)
- [11] Mazierska J and Grabovickic R, 1998 IEEE Trans. on Appl. Supercond. 8 178 - 187
- [12] Szeftel J, Sandeau N and Khater A, 2017 Physics Letters A 381 1525
- [13] Tinkham M 2004 Introduction to Superconductivity 2nd edn (New York: Dover Publications)
- [14] Calatroni S and Vaglio R, 2017 IEEE Trans. on Appl. Supercond. 27 3500506
- [15] Bauer M, Metzger R, Semerad R, Berberich P and Kinder H, 2000 Mat. Res. Soc. Symp. Proc. 585 35
- [16] Lao M, Bernardi J, Bauer M and Eisterer M, 2015 Supercond. Sci. Technol. 28 124002
- [17] Blatter G, Feigelman M V, Geshkenbein V B, Larkin A I and Vinokur V M, 1994 Rev. Mod. Phys. 66 1125
- [18] Prozorov R, Giannetta R W, Carrington A, Fournier P, Greene R L, Guptasarma P, Hinks D G and Banks A R, 2000 Appl. Phys. Lett. 77 4202
- [19] Langan R M, Gordeev S N, Oussena M, de Groot P A J, Jansen A G M, Gagnon R and Taillefer L, 1999 Phys. C 313 294304
- [20] Nakagawa H, Takamasu T, Miura N and Enomoto Y, 1998 Physica B 246 - 247 429
- [21] Gutierrez J, Llordes A, Gazquez J, Gibert M, Roma N, Ricart S, Pomar A, Sandiumenge F, Mestres N and Puig T 2007 Nat. Mater. 6 367
- [22] Gittleman JI and Rosenblum B, 1966 Phys Rev. Lett. 16 734
- [23] Hein M, 1999 High-Temperature Superconductor Thin Films at Microwave Frequencies Springer Berlin
- [24] Marcon R, Fastampa R, Giura M and Silva E, 1991 Phys Rev. B 43 2940
- [25] Rao X S, Ong C K and Feng Y P, 2000 Appl. Phys. Lett. 77 2897
- [26] Chiggiato P, Costa Pinto P, 2006 Thin Solid Films 515 382-388
- [27] Yin Vallgren C, Arduini G, Bauche J, Calatroni S, Chiggiato P, Cornelis K, Costa Pinto P, Henrist B, Mtral E, Neupert H, Rumolo G, Shaposhnikova E. and Taborelli M, 2011 Phys. Rev. ST Accel. Beams 14 071001
- [28] Arduini G, Baglin V, Bruning O, Cappi R, Caspers F, Collier P, Collins I R, Cornelis K, Garoby R, Grobner O, Henrist B, Hilleret N, Hofle W, Jimenez J M, Laurent J-M, Linnecar T, Mercier E, Pivi M, Ruggiero F, Rumolo G, Scheuerlein C, Tuckmantel J, Vos L, Zimmermann F, 2011 proceedings of the LHC Beam Operation workshop, Evian.
- [29] Henrist B, Hilleret N, Scheuerlein C, Taborelli M, 2001 Applied Surface Science 172 95-102

- [30] Giorgi T A, Ferrario B and Storey B, 1998 *Journal of Vacuum Science & Technology* 3 417
- [31] Bean C P, 1962 *Phys. Rev. Lett.* 8 250